Prepared for submission to JCAP

Some correlations in CLASH clusters.

A. Del Popolo[a,b] **K. Umetsu**[a,b] **Xiguo Lee**[a,b]
E-mail: adelpopolo@oact.inaf.it

Abstract. The present paper is a continuation and extension of [1] to CLASH clusters. We study the total, the dark matter density profiles, and correlations in a subgroup of CLASH clusters, as we did for the Newman's clusters. As in the case of Newman clusters, we find that the DM density profile is strongly influenced by interactions with baryons, and the energy and angular momentum transferred from baryons to DM through dynamical friction. The inner slope of the dark matter density profiles of the clusters are usually flatter than the Navarro-Frenk-White profile inner slope, with maximum value -0.79, and minimum -0.30. As in the case of Newman clusters, there are a series of correlations among the slope α of the dark matter profile, and: a. the core radius of clusters; b. the effective radius R_e; c. the mass of the Brightest Central Galaxy (BCG); d. the total baryonic mass, and stellar mass of the clusters. We also found a correlation between the effective radius and the virial mass.

The clusters structure, their total and DM density profiles, and the correlations are understood in a double phase scenario. In the first dissipative phase, the BGC forms. In the second dissipationless phase, the interactions between of baryon cluamps with DM through dynamical friction (DF), flattens the DM distribution. The final result of the two phases is the formation of clusters with different DM distribution, inner slopes, and several correlations between characteristic quantities of the clusters.

Keywords: cosmology, theory, large scale structure of Universe, galaxies, formation

Contents

1 Introduction

The ΛCDM paradigm gives a plethora of correct predictions [1–5], and a series of not correct ones. It predicts that the density profiles of all structures, from dwarf galaxies to clusters is cuspy [6, 7][1]. Observations ([14, 15], and theoretical results [16–21] have shown that the inner slopes of the density profile in dwarf galaxies, and low-surface-brightness galaxies (LSBs), are usually flatter than simulations (the so called cusp-core problem), and there are strong diversity of distribution of DM in similar objects (the so called "diversity problem") [21–23].

Due to the lack of HI the determination of the DM structure in dSPhs, and elliptical galaxies is much more complicated, because of degeneracies related to the mass probes used in the profile determination (see [24]) because of the small dynamic range of observations) . In the case of dSphs there are discrepant results on the cusp-core nature of the density profile [25–28], sometime, even in the case of the same object, studied with different techniques.

Similar uncertainties are present in cluster of galaxies, but they can be overcome in a easier manner than in dSPhs or ellipticals, since in cluster one can combine X-ray observations, lensing and the dynamics of galaxies.

Several studies [29–34], combining different kind of observations found that while the total density profile in clusters is more or less well described by the NFW profile, the inner DM structure is characterized by a flatter inner slope within a radius typical of the BCG radius (from some kpcs to some tens of kpcs). Then, as already reported, the cusp-core problem and the so called diversity problem [21, 23] are also present in clusters of galaxies[2].

As shown by some studies, the quoted discrepancy is eliminated when the results of N-body dissipationless simulations are corrected by taking into account the effects of baryons [17–20, 36–42] Cardone2011,Jardel2009,

In order to study how baryons modify the formation and evolution of clusters, in [43] we used the baryon clumps interacting with DM model introduced in [17] model. Apart finding that baryons mainly concentrated in the inner 10 kpc have an important role in shaping the clusters density profiles, finding correlations of the inner profile from the baryon content, we reproduced some clusters profiles, namely A611, A383, MACS J1423.8+2404, RXJ1133, in agreement with the observational studies of [30–32].

[1] In addition to the quoted problem, the ΛCDM paradigm suffers from the cosmological constant problem [8, 9], the nature of dark energy [10–12] and from several problems at small scales [13]

[2] The scatter in α observed in different galaxies by [22, 35] is also observed in clusters [33, 34].

In [1], we studied MS2137, A963, A383, A611, A2537, A2667, A2390, observed by [33, 34], and reobtaining the correlations found by them, the total mass density profile, well fitted by a NFW pofile, and the DM mass distribution, shallower than the total mass density profile.

The formation picture proposed by [33, 34] is characterized by a dissipational formation of the BCGs, and by a second dissipationless phase. In this phase, similarly to what described by [17, 21, 36, 37, 39, 42–47] baryon clumps interact with DM through dynamical friction "heating" DM and reducing the inner cusp.

Our aim here is to study the CLASH clusters in order to see if we have correlations similar to those observed in the [33, 34] clusters, to study the mass distribution in the clusters, and to verify the "physical picture" proposed by [33, 34], and confirmed in [1].

To this aim we use the data of 16 of the 20 CLASH clusters [48], the unmagnified ones, to repeat an analisys similar to the one performed in [1, 43]. We will reproduce the total masss density profile obtained in [48], by means of a modified version of the model used in [1, 43], taking into account, among other effects, adiabatic contraction responsible of the steepening of the density profiles of clusters in their early phase formation epoch, the interaction between baryonic clumps and DM through dynamical friction, responsible of "heating" the DM component and flattening the density profile, supernovae feedback, AGN feedback and other effects described in detail in the Appendix. The aim is similarly to [1, 33, 34] to check if the total density profile is approximated by a NFW profile or an Einasto's profile, and to see if also in the CLASH clusters we find correlations between the inner slope and the total baryonic content of the clusters, and correlations with other quantities like the effective radius of the BCG, the DM mass, etc.

The plan of the paper is the following. In section 2, we discuss the data used, and give a short qualitative summary of the model. In section 3, we discuss the results, and section 4 is devoted to conclusions.

2 Data used, and summary of the model

The data we use in our analisys comes from a sample of 20 X-ray regular clusters of galaxies with $0.19 \lesssim z \lesssim 0.69$ from which 4 high-magnification clusters were excluded, because they are disturbed merging clusters without a well defined center, chosen from the galaxy clusters at Lensing And Supernova survey with Hubble (CLASH). In particilar, we use the data presented in [48]. The data come from an analysis through weak-lensing shear of the regular clusters, obtained combining wide-field multi-color imaging got with the Subaru Telescope (Suprime-Cam), spanning the cluster radii $10" - 16"$, and 16-band Hubble Space Telescope observations. [48] reconstructed, for each cluster, the surface mass density profile, determinimg their masses and concentrations, in good agreement with the ΛCDM expectations, when taking into account the CLASH selection fuction. [48] obtained an ensemble averaged surface mass density profile, stacking the clusters profiles, which is cuspy, and well described (e.g.) by profiles like the NFW profile, or the Einasto's profiles.

[48] (Table 1) found the radial mass distribution for the quoted 20 CLASH clusters using the weak- and strong-lensing data of [49, 50]. The mass profile solution of each cluster was obtained from a joint likelihood analysis of their weak-lensing shear, strong-lensing, and magnification data. The quoted mass profiles are shown in Fig. 11 of [48]

The estimation of cluster mass,and its radial distribution, can be obtained in different ways. One way is using a Bayesian MCMC approach [48] to obtain an inference of the NFW

density profile (EQ. 2.1),

$$\rho(r) = \frac{\rho_c \delta_c}{r/r_s(1+r/r_s)^2} \tag{2.1}$$

where $r_s = r_{200}/c$ is the scale radius, r_{200} the virial radius c the concentration, being ρ_c the critical density, inside which the mass density of the halo is $200\rho_c$, and

$$\delta_c = \frac{200c^3/3}{\ln(1+c) - c/(1+c)} \tag{2.2}$$

using the data in the form of the discrete cluster mass profile $\mathbf{s} = \mathbf{\Sigma}/\Sigma_{c,\infty}$ and its covariance matrix. The cluster mass profile can be fitted with a $\Sigma(R)_{NFW}$ profile like that of [51] giving a good aproximation to the projected density profile till the virial radius, in the case of cluster-sized haloes [52]. The parameters can be inferred using a χ^2 like that used by [48]

$$\chi^2(\mathbf{p}) = \sum_{i,j}[s_i - \mathbf{s_i}(\mathbf{p})]C_{ij}^{-1}[s_i - \mathbf{s_i}(\mathbf{p})] \tag{2.3}$$

where $\mathbf{p} = (M_{200c}, c_{200c})$, and $\mathbf{s}(\mathbf{p}) = \mathbf{\Sigma}/\Sigma_{c,\infty}$ (see [48])

In the case the surface density profile is not cuspy (e.g. a Singular Isothermal Sphere (SIS)) one needs a an appropriate surfce density, $\Sigma(R)_{SIS}$, for the fit, or the lensing shear in a given radius (see [51]).

As already discussed the density profiles of the 16 CLASH clusters are well approximated by a NFW profile, whose parameters are reported in Table 2 of [48].

In this paper, we will generate clusters having 3 dimensional density pofiles whose surface density profiles are in agreement with those obtained by [48] (Fig. 11). In order to compare with the 2D surface density of [48], starting from the 3 dimensional density profile, $\rho(r)$ we get the surface density integrating $\rho(r)$

$$\Sigma(R) = 2\int_0^\infty \rho(R,z)dz \tag{2.4}$$

being R the projected radius with respect to the cluster center (see also Secs. 5.2, 5.2.2 of [48]).

In order to obtain the 3 dimensional density profile of the clusters, we used a modified version of the model described in [1], qualitatively summarized in the following, and described in the Appendix.

In our model, the protostructure contains baryons and DM. After growing in a linear way, density contrast becomes enough large to stop the prostostructure expansion with Hubble flow, making it recollapse. DM collapse first and baryons follow. Clumps are formed because of radiative processes, and those clumps collapse to the protostructure centre to form stars. At high redshift ($z \simeq 5$ in the case of a protostructure of $10^9 M_\odot$) the collapsing DM compress baryons (adiabatic contraction). The formed clumps transfer energy and angular momentum to DM through dynamical friction. Then DM random motions amplitude increases and DM moves towards the outskirts of the protostructure, with a consequent reduction of the central DM density of the forming structure, and erasing or flattening of the initial cuspy profile. Protostructures giving rise to rotation supported galaxies, suffer a further flattening due to the aquisition of angular momentum in the collapse phase. Supernovae explosions, at later stages $z \simeq 2$ produce expulsion of gas, and the smallest clumps remaining

after star formation are desrupted [42]. AGN feedback has, on larger scales a similar effect to that of SN feedback [40].

The results of our model were compared to the CLASH data as follows.

Using the quoted model, we calculated $\rho(r)$. In [1, 43], the DM density profile had been written as $\rho_{DM} = F(M_{vir}, f_B, j)$, being M_{vir} the cluster virial mass, f_B its baryon content, and j the random angular momentum. In [1, 43], the density profile of the clusters studied was reproduced: a) assuming that the cluster final mass in the model is the same of the observed clusters, b) assuming that the baryon fraction is equal to that calculated by [53] data, and c) adjusting the value of the random angular momentum, to reproduce the observed clusters profiles[3].

In the present paper, the CLASH density profiles were reproduced in a slightly different manner. As in [1, 43], we assumed that the final mass of the protostructures generating one of the CLASH clusters is equal to the known mass of that cluster. The baryonic content, was not fixed as in [1, 43], but the system, initially, has a baryon fraction equal to the universal baryon fraction $f_b = 0.17 \pm 0.01$ [56], and the final baryon fraction was obtained from the star formation processes (see Appendix). The final baryon content, obtained in this way, has been compared with the [53] baryon and gas content in clusters, and was found in agreement with the result of the quoted authors (see also Fig. 1).

The "random" angular momentum was fixed following [57, 58], and to get a better agreement with [48] data, it was slightly modified to obtain a better reproduction (fit) of the CLASH clusters density profiles Differently from [1, 43], the dark matter content was not obtained fitting through the model the total density profile, the baryon profile, and the virial mass. In CLASH clusters, we do not have the DM density profile, or the baryon density profile, but just the total density profile. In order to get the DM profile we subtacted from the total density (given by the data), the baryon density, given by the model.

3 Results and discussion

In [1, 17, 21, 43], we showed how environment, angular momentum, and baryon content influence the characteristics of a structure. The inner density profiles of clusters are flatter in clusters having larger angular momentum [57–64] and larger baryons content (especially in the central region). In [1], we reproduced the total and DM density profiles of [33, 34], and the correlation that those authors found.

The results obtained by [33, 34], and confirmed by our study, are based on strong-lensing, weak-lensing, and improved stellar kinematics with respect to study of the same author or [30]. [34] data allowed the determination of the stellar mass scale, allowing to produce a more physically consistent analysis, reducing the degeneracies among stellar and dark mass, and taking account the BCGs homogeneity. They showed that the total density profile is well approximated by a NFW profile, while the DM profile is usually flatter.

In Fig. 1, we compare the total mass surface density profiles obtained by [48] (dots with error bars) with our model prediction (the three lines, representing the best fit NFW profile (68% CL) to the the observed profile) in the case of A383 (left panel), and A611 (right panel). As shown, our model finely reproduces the [48] surface density, and shows that similarly to what found in [1, 33, 34] that the total mass profile is well approximated by a cuspy profile as

[3]We recall, that clusters of galaxies are non supported by rotation, and then the "ordered" angular momentum, coming from tidal torques, has very similar and low values (some km/s [54, 55]), for all clusters, and in terms of the spin parameter λ can be fixed to the typical value $\lambda = 0.03$ [**?**]

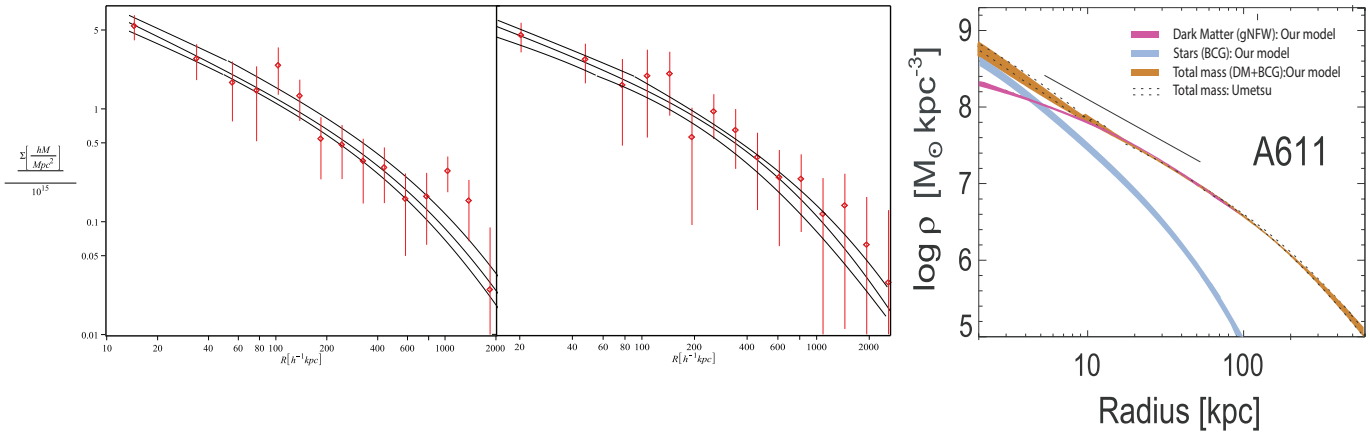

Figure 1. 2 D density profile for A383 (left panel), and A611 (central panel). The dots with error bars are the [48] data, while the central and external lines represent the best fit NFW profile (68% CL) to the observed density profiles. The right panel is the 3 D density profile of A611. The blue, red, and brown bands represent the stars, DM, and total matter density profiles, respectively. The width of the bands indicates the 1 σ uncertainty (see Sect. 4.3 of [34]).

a NFW for both clusters. In the panel c, we show the 3D density profile of one of the clusters A611, obtained with our model. The gray band represents the stars content, the rose one is the DM, the brown one is the total mass, the dashes represent the total mass from the [48] data, and the line is the slope of the NFW profile. The width of the bands indicates the 1σ uncertainties (see Sect. 4.3 of [34]).

Fig. 1 (panel c) shows that the density profiles flattens in the inner region of A611 where the BCG mass starts to be comparable or larger than the DM mass, and this happens in the inner $\simeq 5-10$ kpc (see [34] Fig. 3) (the situation is similar for the other clusters, whose relative plots was not shown). At this radii, the total density profile starts to be steeper than the DM density profile, due to the increase of the role of the baryon mass (mainly the BCG mass) at these radii. At radii $\geq 5-10$ kpc, in the case of all clusters, the total density profile and the DM profile are very close, since DM is dominating on the baryon component. Outside the inner region of the clusters the slope of the total density profiles (and also DM) are comparable in the different clusters. At these radii the DM density profile is in agreement with the NFW profile. At radii ≤ 30 kpc, the total density profile is close to a NFW profile, and as observed by [34] this, somehow, implies a tight coordination among stars distribution and inner DM profile (see the following). Since the total mass (composed by the sum of the DM and the baryonic matter) is well described by a NFW profile, in the quoted inner regions of the cluster, and since the baryonic component is dominant in the 5-10 kpc central region, it is logical to expect that the DM density profile is flatter than a NFW one.

The previous trends are more clearly visible in Fig. 2, and better in Fig. 3, and 4.

In Fig. 2, we plot the inner slope α vs baryon mass (top left panels) and stellar mass (bottom left panels). The dots with errorbars is obtained from a power law fit to the three inner points in the surface density profile. The top left panel represents the α vs baryon mass obtained from the model. The lines representa the ODR fits.

Fig. 2 shows how the 2D slope of the total mass density profile changes with baryon and stellar mass, in the observed clusters (left panels), and in the model (right panels)[4]. The

[4]The smaller error bars of the right panels is due to the smaller errors of the same quantities in the model.

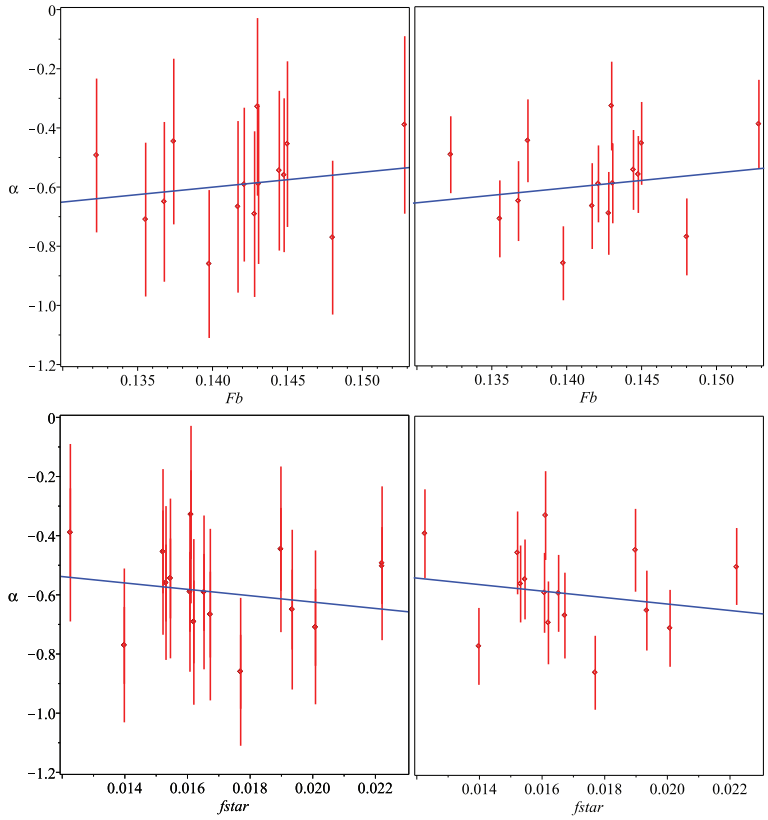

Figure 2. Inner 2 D slope of the total mass density profile vs baryon mass (top left panel) and stellar mass (bottom left panel). The dots with errorbars come from a power law fit of the three inner points in the surface density profile. The top left panel represents the α vs baryon mass obtained from the model, calculating the surface density and then fititng the inner three points with a line. The lines representa the ODR fits.

dots with errorbars were obtained fitting the three inner points??? in the surface density profile with a line. The lines represent the ODR fits to data.

The figure shows a weak correlation between the slope, α, and F_b, and a weak anticorrelation between the slope and f_{stars}. The Spearman correlation coefficient is equal to -0.26 in the case $\alpha - F_b$, and 0.25 in the case $\alpha - f_{stars}$.

This correlation is expected to be weak, since the total mass density profile of each cluster is well approximated by a NFW profile with small scatter, and consequently we have a similar bevavior in the $\alpha - F_b$, $\alpha - f_{stars}$, correlations. We also calculated the correlation between the 3D DM slope and the same quantitiesm which is stronger, and has Spearman coefficients -0.44, and 0.43 respectively. The quoted correlation is stronger because differently from the total mass density profile, the DM profile varies noteworthy from cluster to cluster.

Fig. 3, plots the 3D DM slope, α, vs the BCG mass, M_{BCG}. From the plot it is evident that the larger is the BCG mass of a cluster the flatter is the inner density profile, in agreement with [1, 34, 43]. This is expected since, being the total mass profile well represented by a NFW profile with slope $\simeq -1$, and since the total mass density profile is obtained summing the DM one, and the baryon one, which is dominating DM inside $5-10$ kpc, this implies that the DM profile must be flatter, the steeper is the baryon inner profile. The line represents the orthogonal distance regression (ODR) line, which differently from the linear least-square

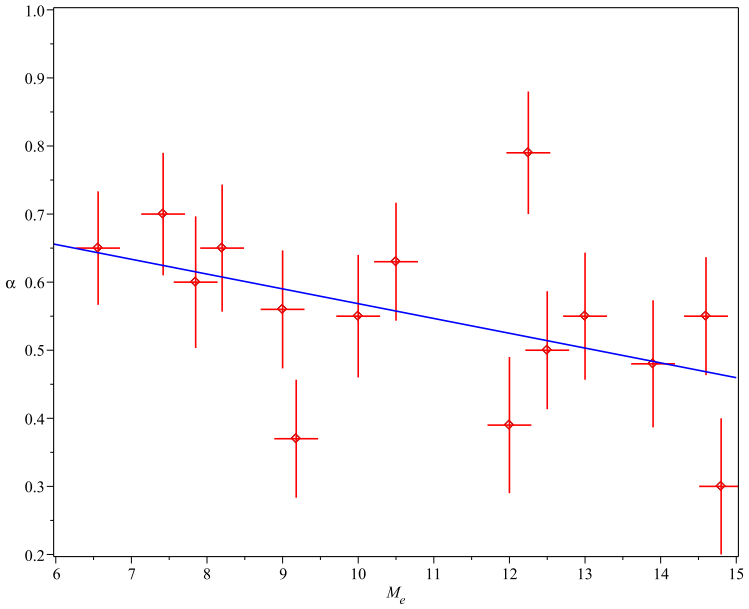

Figure 3. Correlation between the inner slope and the BCG DM mass. The mass of the BCM, M_{BCG}, was obtained using our model. The error on the BCG mass was assumed equal to 0.07 dex [1, 34]. The Spearman rank correlation coefficient is -0.6.

method takes into account the uncertainties in the variables. As in [1, 34], the error on the BCG mass was assumed equal to 0.07 dex. The slope α, was obtained by parameterizing the halo as a generalized NFW model (gNFW). We calculated again the Spearman rank correlation coefficient, which in this case is $\rho = -0.6$, and the P-value $P = 0.02$ testifying for a correlation between α and M_{BCG}.

Differently from Fig. 2, we do not compare the model result with observations, since there is just one study of the CLASH BGGs [65], and it does not study the $\alpha - M_{BCG}$ correlation. The last is studied just for 3 of the CLASH clusters, namely MS2137, A383, A611, by [1, 34]. A comparison of our results with the $\alpha - M_{BCG}$ relation of MS2137, A383, A611 from [1, 34], shows that our $\alpha - M_{BCG}$ is in agreement with them ([34]). Moreover, is to be noticed that a comparison of the BCG mass in [65] with the ones common to [1, 34] (MS2137, A383, A611) shows that [65] estimation are totally different from [34] (except for A383).

In Fig. 4, we plot the correlation $\alpha - R_e$, being R_e the BCG effective radius (radius containing half of the light). [5].

The slope α, was obtained by parameterizing the halo as a generalized NFW model (gNFW). The plot shows that clusters with larger R_e have a shallower inner slope. This correlation is in line with what was previously written. Since a) $M_{DM} = M_{total} - M_{baryon}$, b) the total mass is well described by a NFW profile, and c) a larger BCG contains more baryons, then the DM content is smaller. The line represents the ODR fit, while the Spearman rank correlation coefficient is $\rho = -0.63$ and $P = 0.001159$.

[5]The gNFW is given by

$$\rho_{DM}(r) = \frac{\rho_s}{(r/r_s)^{\alpha}(1 + r/r_s)^{(3-\alpha)}} \tag{3.1}$$

which has a central cusp with $d\log\rho_{DM}/d\log r \to 0$.

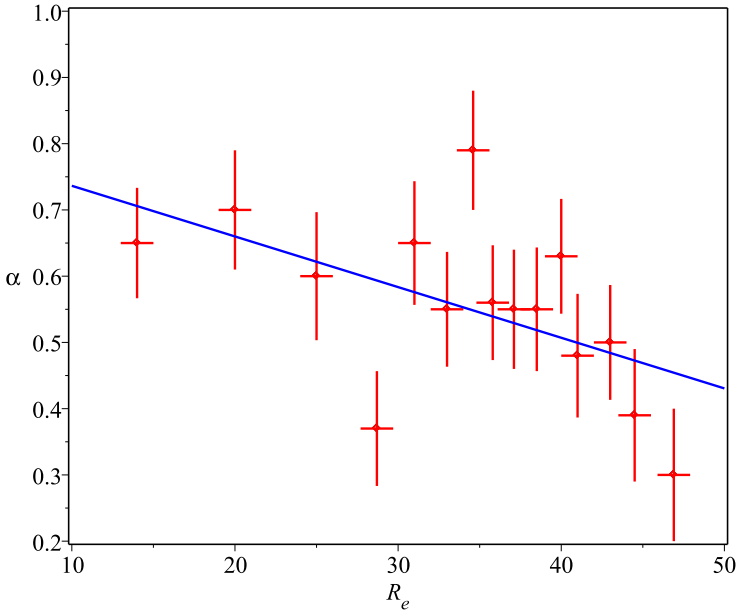

Figure 4. Correlation between the inner slope and the BCG size. The slope was obtaining by fitting a gNFW model to the cluster obtained using our model. The line is the ODR fit to data. The Spearman rank correlation coefficient is $\rho = -0.63$ and $P = 0.001159$.

The plot shows a scatter that is larger than the scatter observed in DM only simulations of clusters, like that of [**?**] (see also the top gray points in [34]). This issue is also present in galaxies, and it has beed dubbed the "diversity problem" [23, 43].

Finally, in Fig. 5, we show the correlation between the effective radius R_e, and the virial mass, M_{500}. The line represents again the ODR fit. The plot shows a positive correlation between the effective radius and the virial mass with a Spearman rank correlation coefficient $\rho = -0.68$, and $P = 0.005$. This is in agreement with previous studies e.g. [66], and in contradiction to [65]. The last authors found no correlation between the BCG mass and the virial mass. They justified this lack of correlation as due to a selection bias in the CLASH sample, due to a selection of clusters having BCGs of small mass. In reality, as previously noticed, the estimate of the BCGs mass by the same authors [65] is strikingly in contrast with the [34] clusters in common with the [65] CLASH sample. Moreover, [65] considered all the CLASH clusters, even the high magnification ones, which, as already reported, are disturbed merging clusters.

The shapes of the density profiles (Fig. 1), the scatter from cluster to cluster as well as the correlations shown in Fig. 3, 4,, can be explained according to our model [17, 21], as follows. At high z, the proto-structure, containing gas and DM, is in its linear phase. The DM mass component collapse before the baryonic mass component, and baryons falls in the DM potential wells, radiating part of their energy, and forming clumps which condense into stars (see [67] (Sect. 2.2.2, 2.2.3)) In the baryon collapse phase, DM is compressed ("adiabatic contraction" (AC))[68, 69] and stars form. This dissipational process, happening at $z \geq 5$ (see [17], Fig. 3, and 5) gives rise to a steep density profile, which constitutes the main structure of the BCG (see also [70, 71]), having a scale radius, $R_e \simeq 30$ kpc, which is similar to the sizes of massive galaxies at high redshift ([72]; [33, 34]). Subsequent merging

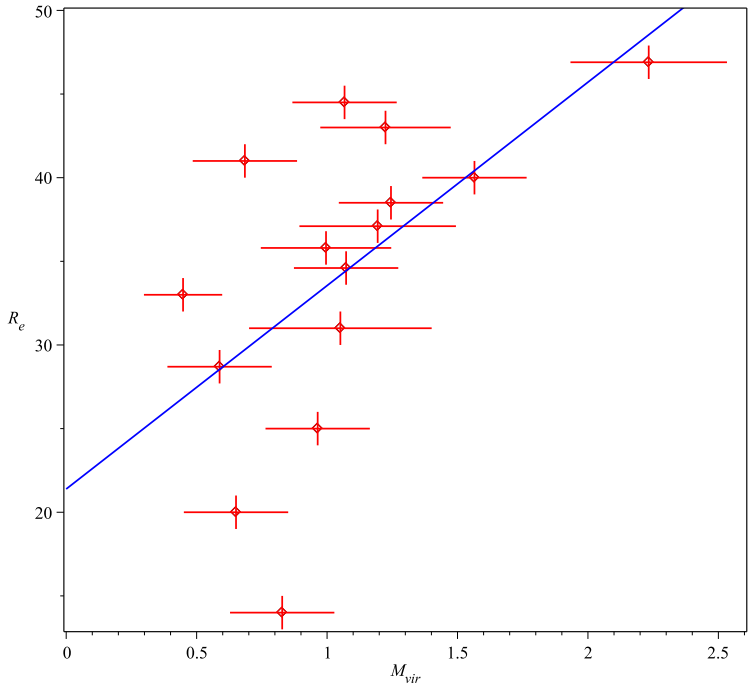

Figure 5. Correlation between R_e and the virial radius. The dashed line is the ODR fit. The Spearman rank correlation coefficient is $\rho = -0.68$ and $P = 0.005$.

of satellites with the proto-BCG adds stars to the outer parts of the BCG (e.g., [73, 74]).

The clumps formed in the baryons collapse phase, moving to the center are exposed to the dynamical friction (DF) from DM particles. The result is a motion of the DM towards the outer parts of the proto-structure reducing the central DM density [17, 36, 37, 39, 42, 47, 75].

Another mechanism proposed to flatten the DM profile is the feedback from AGN (e.g. [40]). However, the process seems to be "too effective", since it produces a core of 10 kpc, which is much larger than what observed [76].

In our scenario, one expects a flattening of the DM density profile, and at the same time an anti-correlation of the inner DM slope, α, with the central baryonic content of the cluster [17, 21, 37]. In our model the density profile shape is regulated by several quantities, and effects: a) angular momentum, b) baryonic fraction, c) virial mass, d) Supernovae and AGN feedback.

The flattening of the inner slope due to the angular momentum is due to the fact that the shells in a proto-structure having larger angular momentum, tend to remain closer to the maximum radius, and consequently they do not contribute to the central density. The flattening of the profile for larger angular momentum was also found by several authors [57, 58, 60–63, 77], and more recently by [78]. The dependence of the slope α on the baryonic mass of the whole cluster, and on the mass contained in the inner 10 kpc was one of the predictions of [21] (see Fig. 2, and Fig. 4b of the quoted paper). The tendency to have flatter profiles for clusters containing larger quantity of baryons, especially at the center, is due to the fact that the larger is the baryonic content of the cluster the larger is the angular momentum transferred from baryons to DM, through DF, with the quoted result that DM particles move away from the cluster center.

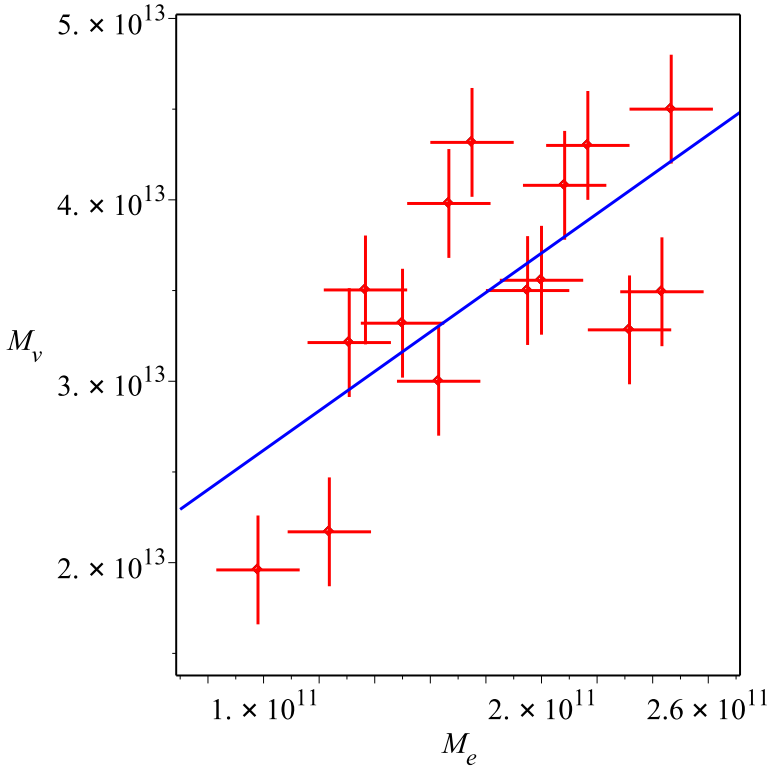

Figure 6. Mass contained in $r < 100$ kpc vs. the mass contained in 5 kpc. Error.....The Spearman rank correlation coefficient is $\rho = 0.64$, $P = 0.011$.

The profile steepens with mass because higher density peaks, characterized by larger ν[6] are statistically the forefathers of more massive haloes, and the last have a larger central density contrast. Consequently, a generic shell will feel a stronger central potential and it will expand less than if the same shell was located in a smaller density peak. The final consequence is a lower quantity of angular momentum acquired in the expansion phase giving rise to haloes more concentrated.

Supernovae and AGN feedback transfer energy to DM particles, moving them on external orbits [40, 79].

In our model the proto-BCG forms at redshift $z \geq 2$, in the dissipative baryonic collapse, and the further evolution of the BCG is due to later merging of stars on the BCG (e.g., [73, 74]). Subsequently, satellites infalling in the halo produces an "heating" of DM, and a flattening of the inner slope ([17, 36, 39, 75]).

Apart the correlations already discussed, in this scenario one expects further correlation among the inner mass of the clusters (5 kpc) mainly constituted by stars, and the mass of the core of the cluster (100 kpc), which at the quoted redshift was already formed, and was subsequently subject to little changes ([80]). In Fig. 5, we compare the mass in the central 5 kpc (mainly stars), and that in 100 kpc (mainly DM). The Spearman rank correlation coefficient is $\rho = 0.64$, $P = 0.011$. As we discuss further in the next section, this can be understood if the innermost regions of the present BCG and cluster halo were in place at

[6] $\nu = \delta(0)/\sigma$, where σ is the mass variance, and δ the fractional density excess in a shell.

early times and changed little in mass subsequently, with accretion mostly adding mass to the outer regions to grow the BCG and the cluster halo.

At the same time it is understood in the picture of the role of baryons in shaping the DM density profile. We showed that the baryonic content was of great importance in shaping the density profile, especially the baryonic content in the central $\simeq$ 10kpc, in the BCG. The cluster final configuration, its content in stars, its BCG characteristics, depends from the initial content of baryons, and by formation process. These considerations lead to think that the BCG mass and the BCG characteristics should be correlated to the baryonic and cluster mass

The previous discussion showed that the DM density profile of the clusters studied has $\alpha < 1$, and that the total density profile is in agreement with a NFW profile.

The results concerning the clusters MS2137, and A383, are consistent with those of [30, 32]. [81] concluded that for any reasonable mass-to-light ratio, the central regions, where the stellar mass is important, are characterized by a shallower DM profile, in agreement with our previous discussions. [82, 83] obtained a value of $\alpha_{\rm DM} = 0.92^{+0.05}_{-0.04}$, considering a fit with a gNFW halo and BCG stars. This slope is similar to that of A611. The cored profiles we found are also in agreement with [40, 41]. The mean slope, we find is $\alpha = 0.54 \pm 0.05$, in agreement with [34].

The inner DM profile is shallower than simulations DM-only simulations. Even considering simulations like [84] the minimum slope obtained, $\alpha \simeq -0.8$ at 120 pc, is larger than the results of observations, and the scatter in the slope from cluster to cluster is much larger than what found in simulations. If some part of the scatter can be explained, in terms of the limits in techniques (e.g., different dynamic ranges in the studies, the BCG role, simplified modeling of clusters) the difference in slope among some clusters is too big to be explained in this way. The discrepancy can be eliminated taking into account baryon physics (dominant in the inner part of clusters) in DM-only simulations. The mechanism described in the Appendix, dynamical friction from baryonic clumps ([17, 36, 39, 45, 75], supernova-AGN-driven flattening ([40, 79] are able to reduce the inner density.

In addition to the astrophysical solution to the problem, other more radical solutions, modifying the particles constituting the DM (e.g., [85–88], modifying the power spectrum at small scales (e.g. [89], considering modified gravity.

Concerning the total density profile, the mean total density profile in our study is $\langle\gamma_{\rm tot}\rangle = 1.05 \pm 0.02$[7], similar to that of [33] ($\langle\gamma_{\rm tot}\rangle = 1.16 \pm 0.05^{+0.05}_{-0.07}$) in the radial range $r = r_{200} \times (0.003 - 0.03)$, in agreement with collisionless DM simulations ([33], Section 9, [7])[8]. [90] found that the profile is NFW-like. [76, 91] found for MACS J1206.2-0847 $\alpha_{\rm tot} = 0.96^{+0.31}_{-0.49}$and for A383 $\alpha_{\rm tot} = 1.08 \pm 0.07$, in agreement with our result (NFW-like profile in $r \gtrsim 5 - 10$ kpc). The stacked density profiles for four clusters studied by [92] gives $\alpha_{\rm tot} = 0.89^{+0.27}_{-0.39}$, when excluding the inner 40 kpc/h.

[7]The average slope of the total mass density profile is calculated as in [33], as $\gamma_{tot} = -\frac{d\log\rho_{tot}}{d\log r}$. The BCG and the DM halo are distinct components, and γ_{tot} is not a directly inferred parameter. It is defined by considering a radial interval, $r = 0.003 - 0.03r_{200}$, and by fitting a line in the plane of $\log r - \log\rho_{tot}$.

[8]It is important to stress that similarly to [33], $\langle\gamma_{\rm tot}\rangle$ is the average slope of the total density profile measured in the radial range $r = r_{200} \times (0.003 - 0.03)$, and is different from α_{tot}, which is the asymptotic inner slopes of gNFW models.

4 Conclusions

In the present paper, similarly to [1], we studied a subsample of CLASH, with the aim of seeing if the DM density profiles of the quoted clusters has similar characteristics to those found in [1, 34], and if CLASH clusters show similar correlations to those of [1, 34].

To this aim, using the M_{500} mass of the clusters given in [48], obtaining the baryonic fraction with the [1, 17**?**] model, and fixing the angular momentum as previously discussed, we reproduced the total mass surface density profiles of the CLASH clusters (except the high magnification ones) in [48]. The total mass 3 D density profile relative to the surface density profile, together with the baryon profile obtained with our model, allow us to obtain the DM profile of the clusters.

The 3 D total mass density profile is characterized by a slope $\langle\gamma_{\rm tot}\rangle = 1.05 \pm 0.02$, in the radius range $r = (0.003 - 0.03) r_{200}$, in agreement with several previous studies (e.g. [33, 34]).

In the radial range $5 - 10$ kpc the total mass is dominated by the star mass, while going towards the clusters outskirts, it is dominated by DM.

This result shows the existence of a tight coordination among the inner DM and the stars distribution, as implied by the fact that the NFW-like profile describing the profile is not generated by DM or baryons only but by their mutual action. The quoted coordination is further supported by the correlation among the mass in 5 kpc and that in 100 kpc (Fig. 6), which indicates that the time-scales of formation of the BCG and the inner cluster are similar. As discussed in [21], the final configuration of a cluster depends from the baryonic content and the formation process. In a hierarchical model of structure formation, we then should expect that the final inner baryonic content and the BCG mass are correlated to the total baryonic and to the mass of the cluster (see [93].

Since the total mass is obtained by summing the DM and baryons content, and moreover since baryons dominate in $5-10$ kpc in the inner 5-10 kpc baryons dominate, the inner density profile slope must be characterized by a slope flatter than that of the total mass density profile, $\alpha < 1$. This is shown in the right panel in fig. 1, and by some of the correlations found. The inner slope of the clusters has values in the rangs -0.79,-0.30,

We also looked for correlations between several of the typical quantities of the clusters (e.g., Re, M_{vir} etc). We found correlations between: a) the 3D inner slope of the DM density profile, α, is anti-correlated with the effective radius, R_e of the clusters. Fig. 3, shows a scatter in the inner slope larger than that observed in DM-only simulations. The scatter is due to the role of the environment as shown in [43]. The anti-correlation is due to the fact that in order total mass have NFW-like profile, clusters having more massive BCGs at their centers must contain less DM in their center. This implies that they must have a flatter DM slope; b) the inner slope of the DM density profile, α and the BCG mass, M_{BCG}, testifying again that larger content of baryons gives ise to flatter DM profiles; c) the virial mass, and the the effective radius, already found in previous studies [66]; d) the mass inside 5 kpc, dominated by baryons, and that inside 100 kpc, dominated by DM[9].

The previous correlations led to conclusion, in agreement with [33, 34], that clusters formed from a dissipative phase, steepening the stellar density profile, and a second dissipationless phase in which the DM density profiles flattened because of the "heating" of DM due to interaction with baryonic clumps through DF ([21, 36, 39, 42, 43, 45, 75].

[9]This is an hint on the early formation of the inner halo and the BCGs, and that accretion played a fundamental role in their formation

Acknowledgements

We would like to thank.....

5 Appendix: the model

The model is a semi-analytical model (SAM) intoduced in [17], used in several papers [1, 19–21, 43], and extended in [**?**]. The model incorporate a secondary infall model (SIM) [58, 63, 94, 95], that differently from previous SIMs take into acount the effect of DM adiabatic contraction [68, 69, 96], those of random and ordered angular momentum [63, 97], and angular momentum transfer between baryons and DM through dynamical friction [17, 19, 36–39, 42].

The model takes into account reionization, cooling, star formation, supernova feedback, and AGN feedback (see the following).

The model follows the evolution of a perturbation starting from the linear phase, expanding with the Hubble flow till the phase of maximum expansion (turn-around).

The final density is given by [98, 99]

$$\rho(x) = \frac{\rho_{ta}(x_m)}{f(x_i)^3}\left[1 + \frac{d\ln f(x_i)}{d\ln x_m(xi)}\right]^{-1} \tag{5.1}$$

where the term $f(x_i) = x/x_m(x_i)$ is the so called collapse factor (see Eq. A18, DP09).

and the turn-around radius with $x_{\rm m}(x_{\rm i})$, given by

$$x_{\rm m} = g(x_{\rm i}) = x_{\rm i}\frac{1+\overline{\delta}_{\rm i}}{\overline{\delta}_{\rm i} - (\Omega_{\rm i}^{-1} - 1)} \ . \tag{5.2}$$

In the previous equation, $\Omega_{\rm i}$ is the density parameter, and $\overline{\delta}_{\rm i}$ the average overdensity in a given shell. Our model contains DM and baryons. Initially, baryons are in the gas phase. Baryon fraction is set equal to the "universal baryon fraction" $f_{\rm b} = 0.17 \pm 0.01$ [56] [0.167 in 2]. The baryonic fraction is obtained from the star formation processes described in the following.

In the model, the "ordered angular momentum" h (coming from tidal torques of large scale structures on those on the smaller scales) is obtained through the tidal torque theory (TTT) [97, 100–103].

A "random" angular momentum, j, is also present in haloes, and is generated by random velocities (Ryden & Gunn 1987). j is expressed in terms of the eccentricity $e = \left(\frac{r_{\rm min}}{r_{\rm max}}\right)$ [57], where $r_{\rm max}$ is the apocentric radius, and $r_{\rm min}$ the pericentric radius. A correction on the eccentricity is made, according to simulations of [58], which consider the effects of the dynamical state of the system on eccentricity

$$e(r_{\rm max}) \simeq 0.8\left(\frac{r_{\rm max}}{r_{\rm ta}}\right)^{0.1} \ , \tag{5.3}$$

for $r_{\rm max} < 0.1 r_{\rm ta}$.

The deceleration term connected to dynamical friction was introduced in the equation of motion (Eq. A14 in DP09). The dynamical friction coefficient was obtained similarly to Antonuccio-Delogu & Colafrancesco (1994) (see also Appendix D of DP09).

The adiabatic contraction (AC) of DM produced by the baryons collapse was taken into account as follows. Our protostructure is made of baryons and DM, baryonic fraction

$F_b = M_b/M_{500} << 1$, and DM fraction $1 - F_b$[10]. Baryons cools and collapse towards the structure center giving rise to a distribution $M_b(r)$. DM is compressed, and particles located initially at r_i move to a new position

$$r\,[M_b(r) + M_{dm}(r)] = r_i M_i(r_i) \tag{5.4}$$

(Blumenthal et al. 1986), being $M_i(r_i)$ the total mass at initial time, and M_{dm} the final distribution of DM. One then assumes that baryons and DM have the same initial distribution (Mo et al. 1998; Cardone & Sereno 2005; Treu & Koopmans 2002; Keeton 2001), and that the final baryon distribution is a Hernquist configuration (Rix et al. 1997; Keeton 2001; Treu & Koopmans 2002). If particles orbits do not cross, we have

$$M_{dm}(r) = (1 - F_b) M_i(r_i) \tag{5.5}$$

Once $M_i(r_i)$ and $M_b(r)$ are given, Eqs. (5.4), (5.5) can be solved to find the final halo distribution. The previous model can be improved assuming that

$$M(\bar{r})r = \text{const.} \tag{5.6}$$

(Gnedin et al. 2004), namely assuming that the product of the mass in the orbit-averaged radius $\bar{r}$ with radius conserves. The quantity

$$\bar{r} = \frac{2}{T_r} \int_{r_{min}}^{r_{max}} r \frac{dr}{v_r}, \tag{5.7}$$

is the orbit-averaged radius, and T_r is the radial period.

Gas cooling, star formation, reionization and supernovae feedback were included as done by [104] and [67] (Sect. 2.2.2 and 2.2.3).

Reionization, treated as in [67], reduces the baryon content, and the baryon fraction changes as

$$f_{\rm b,halo}(z, M_{\rm vir}) = \frac{f_{\rm b}}{[1 + 0.26 M_{\rm F}(z)/M_{\rm vir}]^3}\ , \tag{5.8}$$

where $M_{\rm F}$, is the "filtering mass" [see 105], and as usual the virial mass is indicated as $M_{\rm vir}$. The reionization redshift is in the range 11.5-15.

Gas cooling is treated as a classical cooling flow [e.g., 106] [see Sect. 2.2.2 of 67]. Similar results are obtained using the [97] treatment.

The details of star formation are given in [104]. The treatment of [107] is used for the supernovae feedback. In [108] it was used the blast wave SN feedback (SNF) [109]. For our purposes, the choice of the formalism, even if similar, is not so fundamental. A fundamental difference between our model and the SNF model [e.g., 108] is that in our case the flattening process happens before star formation, and the source of energy is gravitational. Stellar feedback acts when the core is already formed, and disrupts the gas clouds. In the SNFF model the flattening process happens after star formation and the source of energy is stellar feedback.

Concerning these last steps. Gas forms a disc, and the star formation rate is

$$\psi = 0.03 M_{\rm sf}/t_{\rm dyn}\ , \tag{5.9}$$

[10] M_{500} is the mass enclosed in a radius R_{500} within which the density is 500 ρ_c, being ρ_c is the critical density. The total baryonic mass, M_b, is given by the sum of the gas mass, M_{gas}, and the mass in stars, M_*.

being $t_{\rm dyn}$ the disc dynamical time, and $M_{\rm sf}$ the gas mass above a given density threshold, $n > 9.3/cm^3$ as in [108]. The initial mass function (IMF) is a Chabrier one [110]. The amount of stars forming is given by

$$\Delta M_* = \psi \Delta t \ , \tag{5.10}$$

where Δt indicates the time-step.

The quantity of energy injected by SN in the ISM is

$$\Delta E_{\rm SN} = 0.5 \epsilon_{\rm halo} \Delta M_* V_{\rm SN}^2 \ , \tag{5.11}$$

where $V_{\rm SN}^2 = \eta_{\rm SN} E_{\rm SN}$ is the energy injected per supernovae and per unit solar mass. The efficiency reheating disc gas efficiency produced by energy is fixed at $\epsilon_{\rm halo} = 0.35$ [67]. $\eta_{\rm SN} = 8 \times 10^{-3}/M_\odot$ gives the supernovae number per solar mass obtained assuming a Chabrier IMF [110], and the typical energy released in a SN explosion is $E_{\rm SN} = 10^{51}$ erg.

Energy injection in the gas reheats it proportionally to the number of star formed

$$\Delta M_{\rm reheat} = 3.5 \Delta M_* \ . \tag{5.12}$$

The change in thermal energy produced by the reheated gas is given by

$$\Delta E_{\rm hot} = 0.5 \Delta M_{\rm reheat} V_{\rm vir}^2 \ , \tag{5.13}$$

This hot gas will be ejected by the halo if $\Delta E_{\rm SN} > \Delta E_{\rm hot}$, and the quantity is

$$\Delta M_{\rm eject} = \frac{\Delta E_{\rm SN} - \Delta E_{\rm hot}}{0.5 V_{\rm vir}^2} \ . \tag{5.14}$$

The halo can accrete the ejected material that becomes part of the hot component related to the central galaxy [107, 111].

For masses $M \simeq 6 \times 10^{11} M_\odot$, AGN quenching must be taken into account [112]. AGN feedback follows the prescription of [40**?**]. A Super-Massive-Black-Hole (SMBH) is created when the star density exceeds $2.4 \times 10^6 M_\odot/{\rm kpc}^3$, the gas density reaches 10 times the stellar density, and the 3D velocity dispersion exceeds 100 km/s. Each initial (seed) black hole mass starts at 10^5 $M_\odot$. Mass accretion into the SMBH and AGN feedback were implemented modifying the model by [**?**] as in [40].

The model demonstrated its robustness predicting before simulations the density flattening and shape produced by heating of DM, for galaxies [17, 19, 21] in agreement with subsequent SPH simulations [e.g. 18, 113] [see also Fig. 4 of 20, for a direct comparison], and similarly for clusters of galaxies [43] in agreement with hydro-simulations of [41], the inner density slope dependence on the halo mass and on the total baryonic content to the total mass ratio [19, 114], in agreement with [108]. The slope was shown by [19, 114] to depend also on the angular momentum. In [115], the stellar and baryonic Tully-Fisher, Faber-Jackson and the stellar mass vs. halo mass (SMH) relations were shown in agreement with simulations.

Finally, the correct DM profile inner slope dependence on halo mass was explained over 6 order of magnitudes in halo mass, from dwarves to clusters[17, 19, 21, 43], a range no other model achieved.

References

[1] A. Del Popolo, *Nonbaryonic Dark Matter in Cosmology*, *International Journal of Modern Physics D* **23** (Jan., 2014) 30005, [arXiv:1305.0456].

[2] E. Komatsu, K. M. Smith, J. Dunkley, and et al., *Seven-year Wilkinson Microwave Anisotropy Probe (WMAP) Observations: Cosmological Interpretation*, *ApJS* **192** (Feb., 2011) 18–+, [arXiv:1001.4538].

[3] Planck Collaboration, P. A. R. Ade, N. Aghanim, C. Armitage-Caplan, M. Arnaud, M. Ashdown, F. Atrio-Barandela, J. Aumont, C. Baccigalupi, A. J. Banday, and et al., *Planck 2013 results. XVI. Cosmological parameters*, *A& A* **571** (Nov., 2014) A16, [arXiv:1303.5076].

[4] A. Del Popolo, *Non-baryonic dark matter in cosmology*, in *AIP Conf. Proc.*, vol. 1548, pp. 2–63, July, 2013.

[5] A. Del Popolo, *Dark matter, density perturbations, and structure formation*, *Astronomy Reports* **51** (Mar., 2007) 169–196, [arXiv:0801.1091].

[6] J. F. Navarro, C. S. Frenk, and S. D. M. White, *A Universal Density Profile from Hierarchical Clustering*, *ApJ* **490** (Dec., 1997) 493–+, [astro-ph/9611107].

[7] J. F. Navarro, A. Ludlow, V. Springel, J. Wang, M. Vogelsberger, S. D. M. White, A. Jenkins, C. S. Frenk, and A. Helmi, *The diversity and similarity of simulated cold dark matter haloes*, *MNRAS* **402** (Feb., 2010) 21–34, [arXiv:0810.1522].

[8] S. Weinberg, *The cosmological constant problem*, *Reviews of Modern Physics* **61** (Jan., 1989) 1–23.

[9] A. V. Astashenok and A. del Popolo, *Cosmological measure with volume averaging and the vacuum energy problem*, *Classical and Quantum Gravity* **29** (Apr., 2012) 085014, [arXiv:1203.2290].

[10] A. Del Popolo, F. Pace, and J. A. S. Lima, *Extended Spherical Collapse and the Accelerating Universe*, *International Journal of Modern Physics D* **22** (July, 2013) 50038, [arXiv:1207.5789].

[11] A. Del Popolo, F. Pace, and J. A. S. Lima, *Spherical collapse model with shear and angular momentum in dark energy cosmologies*, *MNRAS* **430** (Mar., 2013) 628–637, [arXiv:1212.5092].

[12] A. Del Popolo, F. Pace, S. P. Maydanyuk, J. A. S. Lima, and J. F. Jesus, *Shear and rotation in Chaplygin cosmology*, *PRD* **87** (Feb., 2013) 043527, [arXiv:1303.3628].

[13] A. Del Popolo, F. Pace, and M. Le Delliou, *A high precision semi-analytic mass function*, *JCAP* **3** (Mar., 2017) 032, [arXiv:1703.06918].

[14] B. Moore, *Evidence against dissipation-less dark matter from observations of galaxy haloes*, *Nature* **370** (Aug., 1994) 629–631.

[15] R. A. Flores and J. R. Primack, *Observational and theoretical constraints on singular dark matter halos*, *ApJL* **427** (May, 1994) L1–L4, [astro-ph/9402004].

[16] J. F. Navarro, C. S. Frenk, and S. D. M. White, *The Structure of Cold Dark Matter Halos*, *ApJ* **462** (May, 1996) 563, [astro-ph/9508025].

[17] A. Del Popolo, *The Cusp/Core Problem and the Secondary Infall Model*, *ApJ* **698** (June, 2009) 2093–2113, [arXiv:0906.4447].

[18] F. Governato, C. Brook, L. Mayer, A. Brooks, G. Rhee, J. Wadsley, P. Jonsson, B. Willman, G. Stinson, T. Quinn, and P. Madau, *Bulgeless dwarf galaxies and dark matter cores from supernova-driven outflows*, *Nature* **463** (Jan., 2010) 203–206, [arXiv:0911.2237].

[19] A. Del Popolo, *On the universality of density profiles*, *MNRAS* **408** (Nov., 2010) 1808–1817,

[arXiv:1012.4322].

[20] A. Del Popolo, *Non-power law behavior of the radial profile of phase-space density of halos*, *JCAP* **7** (July, 2011) 14, [arXiv:1112.4185].

[21] A. Del Popolo, *Density profile slopes of dwarf galaxies and their environment*, *MNRAS* **419** (Jan., 2012) 971–984, [arXiv:1105.0090].

[22] J. D. Simon, A. D. Bolatto, A. Leroy, L. Blitz, and E. L. Gates, *High-Resolution Measurements of the Halos of Four Dark Matter-Dominated Galaxies: Deviations from a Universal Density Profile*, *ApJ* **621** (Mar., 2005) 757–776, [astro-ph/0412035].

[23] K. A. Oman, J. F. Navarro, A. Fattahi, C. S. Frenk, T. Sawala, S. D. M. White, R. Bower, R. A. Crain, M. Furlong, M. Schaller, J. Schaye, and T. Theuns, *The unexpected diversity of dwarf galaxy rotation curves*, *MNRAS* **452** (Oct., 2015) 3650–3665, [arXiv:1504.01437].

[24] A. Del Popolo, *On the evolution of aspherical perturbations in the universe: An analytical model*, *A& A* **387** (June, 2002) 759–777, [astro-ph/0202436].

[25] N. C. Amorisco and N. W. Evans, *Dark matter cores and cusps: the case of multiple stellar populations in dwarf spheroidals*, *MNRAS* **419** (Jan., 2012) 184–196, [arXiv:1106.1062].

[26] J. R. Jardel and K. Gebhardt, *The Dark Matter Density Profile of the Fornax Dwarf*, *ApJ* **746** (Feb., 2012) 89, [arXiv:1112.0319].

[27] J. R. Jardel, K. Gebhardt, M. H. Fabricius, N. Drory, and M. J. Williams, *Measuring Dark Matter Profiles Non-Parametrically in Dwarf Spheroidals: An Application to Draco*, *ApJ* **763** (Feb., 2013) 91, [arXiv:1211.5376].

[28] J. R. Jardel and K. Gebhardt, *Variations in a Universal Dark Matter Profile for Dwarf Spheroidals*, *ApJL* **775** (Sept., 2013) L30.

[29] D. J. Sand, T. Treu, and R. S. Ellis, *The Dark Matter Density Profile of the Lensing Cluster MS 2137-23: A Test of the Cold Dark Matter Paradigm*, *ApJL* **574** (Aug., 2002) L129–L133, [astro-ph/0207048].

[30] D. J. Sand, T. Treu, G. P. Smith, and R. S. Ellis, *The Dark Matter Distribution in the Central Regions of Galaxy Clusters: Implications for Cold Dark Matter*, *ApJ* **604** (Mar., 2004) 88–107, [astro-ph/0309465].

[31] A. B. Newman, T. Treu, R. S. Ellis, D. J. Sand, J. Richard, P. J. Marshall, P. Capak, and S. Miyazaki, *The Distribution of Dark Matter Over Three Decades in Radius in the Lensing Cluster Abell 611*, *ApJ* **706** (Dec., 2009) 1078–1094, [arXiv:0909.3527].

[32] A. B. Newman, T. Treu, R. S. Ellis, and D. J. Sand, *The Dark Matter Distribution in A383: Evidence for a Shallow Density Cusp from Improved Lensing, Stellar Kinematic, and X-ray Data*, *ApJL* **728** (Feb., 2011) L39, [arXiv:1101.3553].

[33] A. B. Newman, T. Treu, R. S. Ellis, D. J. Sand, C. Nipoti, J. Richard, and E. Jullo, *The Density Profiles of Massive, Relaxed Galaxy Clusters. I. The Total Density Over Three Decades in Radius*, *ApJ* **765** (Mar., 2013) 24, [arXiv:1209.1391].

[34] A. B. Newman, T. Treu, R. S. Ellis, and D. J. Sand, *The Density Profiles of Massive, Relaxed Galaxy Clusters. II. Separating Luminous and Dark Matter in Cluster Cores*, *ApJ* **765** (Mar., 2013) 25, [arXiv:1209.1392].

[35] W. J. G. de Blok, F. Walter, E. Brinks, C. Trachternach, S.-H. Oh, and R. C. Kennicutt, Jr., *High-Resolution Rotation Curves and Galaxy Mass Models from THINGS*, *AJ* **136** (Dec., 2008) 2648–2719, [arXiv:0810.2100].

[36] A. A. El-Zant, Y. Hoffman, J. Primack, F. Combes, and I. Shlosman, *Flat-cored Dark Matter in Cuspy Clusters of Galaxies*, *ApJL* **607** (June, 2004) L75–L78, [astro-ph/0309412].

[37] C. Nipoti, T. Treu, L. Ciotti, and M. Stiavelli, *Galactic cannibalism and cold dark matter*

density profiles, *MNRAS* **355** (Dec., 2004) 1119–1124, [astro-ph/0404127].

[38] A. Del Popolo and P. Kroupa, *Density profiles of dark matter haloes on galactic and cluster scales*, *A& A* **502** (Aug., 2009) 733–747, [arXiv:0906.1146].

[39] D. R. Cole, W. Dehnen, and M. I. Wilkinson, *Weakening dark matter cusps by clumpy baryonic infall*, *MNRAS* **416** (Sept., 2011) 1118–1134, [arXiv:1105.4050].

[40] D. Martizzi, R. Teyssier, B. Moore, and T. Wentz, *The effects of baryon physics, black holes and active galactic nucleus feedback on the mass distribution in clusters of galaxies*, *MNRAS* **422** (June, 2012) 3081–3091, [arXiv:1112.2752].

[41] D. Martizzi, R. Teyssier, and B. Moore, *Cusp-core transformations induced by AGN feedback in the progenitors of cluster galaxies*, *MNRAS* **432** (July, 2013) 1947–1954, [arXiv:1211.2648].

[42] C. Nipoti and J. Binney, *Early flattening of dark matter cusps in dwarf spheroidal galaxies*, *MNRAS* **446** (Jan., 2015) 1820–1828, [arXiv:1410.6169].

[43] A. Del Popolo, *On the density-profile slope of clusters of galaxies*, *MNRAS* **424** (July, 2012) 38–51, [arXiv:1204.4439].

[44] C.-P. Ma and M. Boylan-Kolchin, *Are Halos of Collisionless Cold Dark Matter Collisionless?*, *Physical Review Letters* **93** (July, 2004) 021301, [astro-ph/0403102].

[45] E. Romano-Díaz, I. Shlosman, Y. Hoffman, and C. Heller, *Erasing Dark Matter Cusps in Cosmological Galactic Halos with Baryons*, *ApJL* **685** (Oct., 2008) L105–L108, [arXiv:0808.0195].

[46] E. Romano-Díaz, I. Shlosman, C. Heller, and Y. Hoffman, *Dissecting Galaxy Formation. I. Comparison Between Pure Dark Matter and Baryonic Models*, *ApJ* **702** (Sept., 2009) 1250–1267, [arXiv:0901.1317].

[47] S. Inoue and T. R. Saitoh, *Cores and revived cusps of dark matter haloes in disc galaxy formation through clump clusters*, *MNRAS* **418** (Dec., 2011) 2527–2531, [arXiv:1108.0906].

[48] K. Umetsu, A. Zitrin, D. Gruen, J. Merten, M. Donahue, and M. Postman, *CLASH: Joint Analysis of Strong-lensing, Weak-lensing Shear, and Magnification Data for 20 Galaxy Clusters*, *ApJ* **821** (Apr., 2016) 116, [arXiv:1507.04385].

[49] K. Umetsu, E. Medezinski, M. Nonino, J. Merten, M. Postman, M. Meneghetti, M. Donahue, N. Czakon, A. Molino, S. Seitz, D. Gruen, D. Lemze, I. Balestra, N. Bentez, A. Biviano, T. Broadhurst, H. Ford, C. Grillo, A. Koekemoer, P. Melchior, A. Mercurio, J. Moustakas, P. Rosati, and A. Zitrin, *Clash: Weak-lensing shear-and-magnification analysis of 20 galaxy clusters*, *The Astrophysical Journal* **795** (2014), no. 2 163.

[50] A. Zitrin, A. Fabris, J. Merten, P. Melchior, M. Meneghetti, A. Koekemoer, D. Coe, M. Maturi, M. Bartelmann, M. Postman, K. Umetsu, G. Seidel, I. Sendra, T. Broadhurst, I. Balestra, A. Biviano, C. Grillo, A. Mercurio, M. Nonino, P. Rosati, L. Bradley, M. Carrasco, M. Donahue, H. Ford, B. L. Frye, and J. Moustakas, *Hubble space telescope combined strong and weak lensing analysis of the clash sample: Mass and magnification models and systematic uncertainties*, *The Astrophysical Journal* **801** (2015), no. 1 44.

[51] C. O. Wright and T. G. Brainerd, *Gravitational Lensing by NFW Halos*, *ApJ* **534** (May, 2000) 34–40.

[52] M. Oguri and T. Hamana, *Detailed cluster lensing profiles at large radii and the impact on cluster weak lensing studies*, *MNRAS* **414** (July, 2011) 1851–1861, [arXiv:1101.0650].

[53] S. Giodini, D. Pierini, A. Finoguenov, G. W. Pratt, H. Boehringer, A. Leauthaud, L. Guzzo, H. Aussel, M. Bolzonella, P. Capak, M. Elvis, G. Hasinger, O. Ilbert, J. S. Kartaltepe, A. M. Koekemoer, S. J. Lilly, R. Massey, H. J. McCracken, J. Rhodes, M. Salvato, D. B. Sanders,

N. Z. Scoville, S. Sasaki, V. Smolcic, Y. Taniguchi, D. Thompson, and COSMOS Collaboration, *Stellar and Total Baryon Mass Fractions in Groups and Clusters Since Redshift 1*, *ApJ* **703** (Sept., 2009) 982–993, [arXiv:0904.0448].

[54] P. Catelan and T. Theuns, *Evolution of the angular momentum of protogalaxies from tidal torques: Zel'dovich approximation*, *MNRAS* **282** (Sept., 1996) 436–454, [astro-ph/9].

[55] P. Catelan and T. Theuns, *Non-linear evolution of the angular momentum of protostructures from tidal torques*, *MNRAS* **282** (Sept., 1996) 455–469, [astro-ph/9].

[56] E. Komatsu, J. Dunkley, M. R. Nolta, and et al., *Five-Year Wilkinson Microwave Anisotropy Probe Observations: Cosmological Interpretation*, *ApJS* **180** (Feb., 2009) 330–376, [arXiv:0803.0547].

[57] V. Avila-Reese, C. Firmani, and X. Hernández, *On the Formation and Evolution of Disk Galaxies: Cosmological Initial Conditions and the Gravitational Collapse*, *ApJ* **505** (Sept., 1998) 37–49, [astro-ph/9710201].

[58] Y. Ascasibar, G. Yepes, S. Gottlöber, and V. Müller, *On the physical origin of dark matter density profiles*, *MNRAS* **352** (Aug., 2004) 1109–1120, [astro-ph/0].

[59] K. Subramanian, R. Cen, and J. P. Ostriker, *The Structure of Dark Matter Halos in Hierarchical Clustering Theories*, *ApJ* **538** (Aug., 2000) 528–542, [astro-ph/9].

[60] A. Nusser, *Self-similar spherical collapse with non-radial motions*, *MNRAS* **325** (Aug., 2001) 1397–1401, [astro-ph/0008217].

[61] N. Hiotelis, *Density profiles in a spherical infall model with non-radial motions*, *A& A* **382** (Jan., 2002) 84–91, [astro-ph/0].

[62] M. Le Delliou and R. N. Henriksen, *Non-radial motion and the NFW profile*, *A& A* **408** (Sept., 2003) 27–38, [astro-ph/0].

[63] L. L. R. Williams, A. Babul, and J. J. Dalcanton, *Investigating the Origins of Dark Matter Halo Density Profiles*, *ApJ* **604** (Mar., 2004) 18–39, [astro-ph/0312002].

[64] Y. Ascasibar, P. Jean, C. Bœhm, and J. Knödlseder, *Constraints on dark matter and the shape of the Milky Way dark halo from the 511-keV line*, *MNRAS* **368** (June, 2006) 1695–1705, [astro-ph/0507142].

[65] C. Burke, M. Hilton, and C. Collins, *Coevolution of brightest cluster galaxies and intracluster light using CLASH*, *MNRAS* **449** (May, 2015) 2353–2367, [arXiv:1503.04321].

[66] A. V. Kravtsov, *The Size-Virial Radius Relation of Galaxies*, *ApJL* **764** (Feb., 2013) L31, [arXiv:1212.2980].

[67] Y.-S. Li, G. De Lucia, and A. Helmi, *On the nature of the Milky Way satellites*, *MNRAS* **401** (Jan., 2010) 2036–2052, [arXiv:0909.1291].

[68] G. R. Blumenthal, S. M. Faber, R. Flores, and J. R. Primack, *Contraction of dark matter galactic halos due to baryonic infall*, *ApJ* **301** (Feb., 1986) 27–34.

[69] O. Y. Gnedin, A. V. Kravtsov, A. A. Klypin, and D. Nagai, *Response of Dark Matter Halos to Condensation of Baryons: Cosmological Simulations and Improved Adiabatic Contraction Model*, *ApJ* **616** (Nov., 2004) 16–26, [astro-ph/0406247].

[70] A. Immeli, M. Samland, O. Gerhard, and P. Westera, *Gas physics, disk fragmentation, and bulge formation in young galaxies*, *A& A* **413** (Jan., 2004) 547–561, [astro-ph/0312139].

[71] C. N. Lackner and J. P. Ostriker, *Dissipational Versus Dissipationless Galaxy Formation and the Dark Matter Content of Galaxies*, *ApJ* **712** (Mar., 2010) 88–100, [arXiv:1002.0585].

[72] I. Trujillo, N. M. Förster Schreiber, G. Rudnick, M. Barden, M. Franx, H.-W. Rix, J. A. R. Caldwell, D. H. McIntosh, S. Toft, B. Häussler, A. Zirm, P. G. van Dokkum, I. Labbé,

A. Moorwood, H. Röttgering, A. van der Wel, P. van der Werf, and L. van Starkenburg, *The Size Evolution of Galaxies since z˜3: Combining SDSS, GEMS, and FIRES*, *ApJ* **650** (Oct., 2006) 18–41, [astro-ph/0504225].

[73] T. Naab, P. H. Johansson, and J. P. Ostriker, *Minor Mergers and the Size Evolution of Elliptical Galaxies*, *ApJL* **699** (July, 2009) L178–L182, [arXiv:0903.1636].

[74] C. F. P. Laporte, S. D. M. White, T. Naab, M. Ruszkowski, and V. Springel, *Shallow dark matter cusps in galaxy clusters*, *MNRAS* **424** (July, 2012) 747–753, [arXiv:1202.2357].

[75] A. El-Zant, I. Shlosman, and Y. Hoffman, *Dark Halos: The Flattening of the Density Cusp by Dynamical Friction*, *ApJ* **560** (Oct., 2001) 636–643, [astro-ph/0103386].

[76] M. Postman, T. R. Lauer, M. Donahue, G. Graves, D. Coe, J. Moustakas, A. Koekemoer, L. Bradley, H. C. Ford, C. Grillo, A. Zitrin, D. Lemze, T. Broadhurst, L. Moustakas, B. Ascaso, E. Medezinski, and D. Kelson, *A Brightest Cluster Galaxy with an Extremely Large Flat Core*, *ApJ* **756** (Sept., 2012) 159, [arXiv:1205.3839].

[77] P. Sikivie, I. I. Tkachev, and Y. Wang, *Secondary infall model of galactic halo formation and the spectrum of cold dark matter particles on Earth*, *PRD* **56** (Aug., 1997) 1863–1878, [astro-ph/9].

[78] E. Polisensky and M. Ricotti, *Fingerprints of the initial conditions on the density profiles of cold and warm dark matter haloes*, *MNRAS* **450** (June, 2015) 2172–2184, [arXiv:1504.02126].

[79] A. Pontzen and F. Governato, *Cold dark matter heats up*, *Nature* **506** (Feb., 2014) 171–178, [arXiv:1402.1764].

[80] L. Gao, A. Loeb, P. J. E. Peebles, S. D. M. White, and A. Jenkins, *Early Formation and Late Merging of the Giant Galaxies*, *ApJ* **614** (Oct., 2004) 17–25, [astro-ph/0312499].

[81] L. Zappacosta, D. A. Buote, F. Gastaldello, P. J. Humphrey, J. Bullock, F. Brighenti, and W. Mathews, *The Absence of Adiabatic Contraction of the Radial Dark Matter Profile in the Galaxy Cluster A2589*, *ApJ* **650** (Oct., 2006) 777–790, [astro-ph/0602613].

[82] M. Limousin, J. Richard, J.-P. Kneib, H. Brink, R. Pelló, E. Jullo, H. Tu, J. Sommer-Larsen, E. Egami, M. J. Michałowski, R. Cabanac, and D. P. Stark, *Strong lensing in Abell 1703: constraints on the slope of the inner dark matter distribution*, *A& A* **489** (Oct., 2008) 23–35, [arXiv:0802.4292].

[83] J. Richard, L. Pei, M. Limousin, E. Jullo, and J. P. Kneib, *Keck spectroscopic survey of strongly lensed galaxies in Abell 1703: further evidence of a relaxed, unimodal cluster*, *A& A* **498** (Apr., 2009) 37–47, [arXiv:0901.0427].

[84] J. Stadel, D. Potter, B. Moore, J. Diemand, P. Madau, M. Zemp, M. Kuhlen, and V. Quilis, *Quantifying the heart of darkness with GHALO - a multibillion particle simulation of a galactic halo*, *MNRAS* **398** (Sept., 2009) L21–L25, [arXiv:0808.2981].

[85] P. Colín, V. Avila-Reese, and O. Valenzuela, *Substructure and Halo Density Profiles in a Warm Dark Matter Cosmology*, *ApJ* **542** (Oct., 2000) 622–630, [astro-ph/0004115].

[86] J. Sommer-Larsen and A. Dolgov, *Formation of Disk Galaxies: Warm Dark Matter and the Angular Momentum Problem*, *ApJ* **551** (Apr., 2001) 608–623, [astro-ph/9912166].

[87] P. J. E. Peebles, *Fluid Dark Matter*, *ApJL* **534** (May, 2000) L127–L129, [astro-ph/0002495].

[88] M. Kaplinghat, L. Knox, and M. S. Turner, *Annihilating Cold Dark Matter*, *Physical Review Letters* **85** (Oct., 2000) 3335, [astro-ph/0005210].

[89] A. R. Zentner and J. S. Bullock, *Halo Substructure and the Power Spectrum*, *ApJ* **598** (Nov., 2003) 49–72, [astro-ph/0304292].

[90] D. Coe, K. Umetsu, A. Zitrin, M. Donahue, E. Medezinski, M. Postman, M. Carrasco,

T. Anguita, M. J. Geller, K. J. Rines, A. Diaferio, M. J. Kurtz, L. Bradley, A. Koekemoer, W. Zheng, M. Nonino, A. Molino, A. Mahdavi, D. Lemze, L. Infante, S. Ogaz, P. Melchior, O. Host, H. Ford, C. Grillo, P. Rosati, Y. Jiménez-Teja, J. Moustakas, T. Broadhurst, B. Ascaso, O. Lahav, M. Bartelmann, N. Benítez, R. Bouwens, O. Graur, G. Graves, S. Jha, S. Jouvel, D. Kelson, L. Moustakas, D. Maoz, M. Meneghetti, J. Merten, A. Riess, S. Rodney, and S. Seitz, *CLASH: Precise New Constraints on the Mass Profile of the Galaxy Cluster A2261*, *ApJ* **757** (Sept., 2012) 22, [arXiv:1201.1616].

[91] A. Zitrin, T. Broadhurst, D. Coe, K. Umetsu, M. Postman, N. Benítez, M. Meneghetti, E. Medezinski, S. Jouvel, L. Bradley, A. Koekemoer, W. Zheng, H. Ford, J. Merten, D. Kelson, O. Lahav, D. Lemze, A. Molino, M. Nonino, M. Donahue, P. Rosati, A. Van der Wel, M. Bartelmann, R. Bouwens, O. Graur, G. Graves, O. Host, L. Infante, S. Jha, Y. Jimenez-Teja, R. Lazkoz, D. Maoz, C. McCully, P. Melchior, L. A. Moustakas, S. Ogaz, B. Patel, E. Regoes, A. Riess, S. Rodney, and S. Seitz, *The Cluster Lensing and Supernova Survey with Hubble (CLASH): Strong-lensing Analysis of A383 from 16-band HST/WFC3/ACS Imaging*, *ApJ* **742** (Dec., 2011) 117, [arXiv:1103.5618].

[92] K. Umetsu, T. Broadhurst, A. Zitrin, E. Medezinski, D. Coe, and M. Postman, *A Precise Cluster Mass Profile Averaged from the Highest-quality Lensing Data*, *ApJ* **738** (Sept., 2011) 41, [arXiv:1105.0444].

[93] I. M. Whiley, A. Aragón-Salamanca, G. De Lucia, A. von der Linden, S. P. Bamford, P. Best, M. N. Bremer, P. Jablonka, O. Johnson, B. Milvang-Jensen, S. Noll, B. M. Poggianti, G. Rudnick, R. Saglia, S. White, and D. Zaritsky, *The evolution of the brightest cluster galaxies since z ˜ 1 from the ESO Distant Cluster Survey (EDisCS)*, *MNRAS* **387** (July, 2008) 1253–1263, [arXiv:0804.2152].

[94] J. E. Gunn and J. R. Gott, III, *On the Infall of Matter Into Clusters of Galaxies and Some Effects on Their Evolution*, *ApJ* **176** (Aug., 1972) 1.

[95] Y. Hoffman and J. Shaham, *Local density maxima - Progenitors of structure*, *ApJ* **297** (Oct., 1985) 16–22.

[96] M. Gustafsson, M. Fairbairn, and J. Sommer-Larsen, *Baryonic pinching of galactic dark matter halos*, *PRD* **74** (Dec., 2006) 123522, [astro-ph/0608634].

[97] B. S. Ryden, *Galaxy formation - The role of tidal torques and dissipational infall*, *ApJ* **329** (June, 1988) 589–611.

[98] J. E. Gunn, *Massive galactic halos. I - Formation and evolution*, *ApJ* **218** (Dec., 1977) 592–598.

[99] J. A. Fillmore and P. Goldreich, *Self-similar gravitational collapse in an expanding universe*, *ApJ* **281** (June, 1984) 1–8.

[100] F. Hoyle, *On the Fragmentation of Gas Clouds Into Galaxies and Stars.*, *ApJ* **118** (Nov., 1953) 513.

[101] P. J. E. Peebles, *Origin of the Angular Momentum of Galaxies*, *ApJ* **155** (Feb., 1969) 393.

[102] S. D. M. White, *Angular momentum growth in protogalaxies*, *ApJ* **286** (Nov., 1984) 38–41.

[103] D. J. Eisenstein and A. Loeb, *An analytical model for the triaxial collapse of cosmological perturbations*, *ApJ* **439** (Feb., 1995) 520–541, [astro-ph/9].

[104] G. De Lucia and A. Helmi, *The Galaxy and its stellar halo: insights on their formation from a hybrid cosmological approach*, *MNRAS* **391** (Nov., 2008) 14–31, [arXiv:0804.2465].

[105] A. V. Kravtsov, O. Y. Gnedin, and A. A. Klypin, *The Tumultuous Lives of Galactic Dwarfs and the Missing Satellites Problem*, *ApJ* **609** (July, 2004) 482–497, [astro-ph/0401088].

[106] S. D. M. White and C. S. Frenk, *Galaxy formation through hierarchical clustering*, *ApJ* **379**

(Sept., 1991) 52–79.

[107] D. J. Croton, V. Springel, S. D. M. White, G. De Lucia, C. S. Frenk, L. Gao, A. Jenkins, G. Kauffmann, J. F. Navarro, and N. Yoshida, *The many lives of active galactic nuclei: cooling flows, black holes and the luminosities and colours of galaxies*, *MNRAS* **365** (Jan., 2006) 11–28, [astro-ph/0508046].

[108] A. Di Cintio, C. B. Brook, A. V. Macciò, G. S. Stinson, A. Knebe, A. A. Dutton, and J. Wadsley, *The dependence of dark matter profiles on the stellar-to-halo mass ratio: a prediction for cusps versus cores*, *MNRAS* **437** (Jan., 2014) 415–423, [arXiv:1306.0898].

[109] G. Stinson, A. Seth, N. Katz, J. Wadsley, F. Governato, and T. Quinn, *Star formation and feedback in smoothed particle hydrodynamic simulations - I. Isolated galaxies*, *MNRAS* **373** (Dec., 2006) 1074–1090, [astro-ph/0602350].

[110] G. Chabrier, *Galactic Stellar and Substellar Initial Mass Function*, *PASP* **115** (July, 2003) 763–795, [astro-ph/0304382].

[111] G. De Lucia, G. Kauffmann, and S. D. M. White, *Chemical enrichment of the intracluster and intergalactic medium in a hierarchical galaxy formation model*, *MNRAS* **349** (Apr., 2004) 1101–1116, [astro-ph/0310268].

[112] A. Cattaneo, A. Dekel, J. Devriendt, B. Guiderdoni, and J. Blaizot, *Modelling the galaxy bimodality: shutdown above a critical halo mass*, *MNRAS* **370** (Aug., 2006) 1651–1665, [astro-ph/0601295].

[113] F. Governato, A. Zolotov, A. Pontzen, C. Christensen, S. H. Oh, A. M. Brooks, T. Quinn, S. Shen, and J. Wadsley, *Cuspy no more: how outflows affect the central dark matter and baryon distribution in* Λ *cold dark matter galaxies*, *MNRAS* **422** (May, 2012) 1231–1240, [arXiv:1202.0554].

[114] A. Del Popolo and F. Pace, *The Cusp/Core problem: supernovae feedback versus the baryonic clumps and dynamical friction model*, *Ap&SS* **361** (May, 2016) 162, [arXiv:1502.01947].

[115] A. Del Popolo, *On the dark matter haloes inner structure and galaxy morphology*, *Ap&SS* **361** (July, 2016) 222, [arXiv:1607.07408].